LETTERS
PUBLISHED ONLINE: 26 JANUARY 2015 | DOI: 10.1038/NPHYS3201
nature physics

Magnetic control of valley pseudospin in monolayer WSe_2

G. Aivazian[1], Zhirui Gong[2], Aaron M. Jones[1], Rui-Lin Chu[3], J. Yan[4,5], D. G. Mandrus[4,5,6], Chuanwei Zhang[3], David Cobden[1], Wang Yao[2]* and X. Xu[1,7]*

Local energy extrema of the bands in momentum space, or valleys, can endow electrons in solids with pseudospin in addition to real spin[1-5]. In transition metal dichalcogenides this valley pseudospin, like real spin, is associated with a magnetic moment[1,6] that underlies the valley-dependent circular dichroism[6] that allows optical generation of valley polarization[7-9], intervalley quantum coherence[10] and the valley Hall effect[11]. However, magnetic manipulation of valley pseudospin via this magnetic moment[12,13], analogous to what is possible with real spin, has not been shown before. Here we report observation of the valley Zeeman splitting and magnetic tuning of polarization and coherence of the excitonic valley pseudospin, by performing polarization-resolved magneto-photoluminescence on monolayer WSe_2. Our measurements reveal both the atomic orbital and lattice contributions to the valley orbital magnetic moment; demonstrate the deviation of the band edges in the valleys from an exact massive Dirac fermion model; and reveal a striking difference between the magnetic responses of neutral and charged valley excitons that is explained by renormalization of the excitonic spectrum due to strong exchange interactions.

In monolayer transition metal dichalcogenides (TMDs), there is a valley pseudospin 1/2 which describes the two inequivalent but energy-degenerate band edges (the ±K valleys) at the corners of the hexagonal Brillouin zone[1]. With broken inversion symmetry, electrons in the two valleys can have finite orbital contributions to their magnetic moments which are equal in magnitude but opposite in sign by time-reversal symmetry. This orbital magnetic moment is thus linked to the valley pseudospin in the same way that the bare magnetic moment ($g\mu_B\mathbf{S}$) is linked to the real spin $\mathbf{S}$, where μ_B is the Bohr magneton and g is the Lande g-factor. The orbital magnetic moment in turn has two parts: a contribution from the parent atomic orbitals, and a 'valley magnetic moment' contribution from the lattice structure[1] (Fig. 1a, top). The latter is related to the Berry curvature that produces the valley Hall effect[11].

The valley magnetic moment results in a valley-dependent optical selection rule in monolayer TMDs, where light of σ^+ (σ^-) circular polarization excites electron–hole pairs exclusively in the +K (−K) valley. This enables optical manipulation of the valley pseudospin through its excitonic states[7–10,14–17], or valley excitons. The neutral and charged valley excitons, with their exceptionally strong Coulomb interaction[18–24], are subject to a momentum-dependent gauge field arising from electron–hole exchange, or valley–orbit coupling, which at zero magnetic field is predicted to result in massless and massive dispersion, respectively, within the light cone[25]. This implies the possibility of controlling excitonic valley pseudospin via the Zeeman effect in an external magnetic field.

Our measurements of polarization-resolved photoluminescence (PL) in a magnetic field perpendicular to the 2D plane are performed on mechanically exfoliated WSe_2 monolayers. We have obtained consistent results from many samples. The data presented here are all taken from one sample at a temperature of 30 K. To resolve the splitting between the +K and −K valley excitons, which is significantly smaller than the exciton linewidth (∼10 meV), we both excite and detect with a single helicity of light. In this way we address one valley at a time, and the splitting can be determined by comparing the peak positions for different polarizations.

Figure 1b shows the normalized PL spectra for the neutral exciton peak at selected values of the magnetic field B. At zero field (middle) the PL from the +K valley exciton (blue, σ^+) is identical to that from the −K valley (red, σ^-), as expected from time-reversal symmetry[10]. In contrast, at high field the σ^+ and σ^- components are split, with σ^- at a slightly higher energy than σ^+ for +7 T (top) and lower for −7 T (bottom). The small variations in lineshape seen here in the σ^- emission are artefacts related to sample inhomogeneity. To minimize their effect we extract the splitting in two ways (see Supplementary Methods 1), neither of which involves fitting the peaks. The results of both are shown in Fig. 1c. The black squares are obtained from the maximal points of the peaks, whereas the red circles are obtained from their 'centre of mass'. These two very different methods both yield a similar splitting proportional to B. The error bar also shown corresponds to the spectral resolution of the detection system. For a conservative estimate of the slope, we fit the rougher 'max point' data to a straight line, yielding a slope of $-0.11 \pm 0.01\ \mathrm{meV\,T^{-1}} = -(1.9 \pm 0.2)\,\mu_B$.

The observed magnetic spectral splitting can be explained by the combination of the magnetic moment of the tungsten d-orbitals[26] and the 'valley magnetic moment' m_τ, the lattice contribution associated with Berry curvature[6]. The bottom panel of Fig. 1a shows the Zeeman shift of the band edges from each of these two contributions as well as that from the bare spin. The dashed (solid) lines are the conduction and valence band edges at zero (positive) magnetic field, with blue and red denoting spin up and down, respectively. Because of the giant spin splitting (∼0.4 eV) in the valence band, the valence band edge in the +K (−K) valley has only spin-up (down) states. For the conduction band edge, on the other hand, the spin splitting is small (∼0.03 eV), with opposite sign in

[1]Department of Physics, University of Washington, Seattle, Washington 98195, USA. [2]Department of Physics and Center of Theoretical and Computational Physics, University of Hong Kong, Hong Kong, China. [3]Department of Physics, The University of Texas at Dallas, Richardson, Texas 75080, USA. [4]Materials Science and Technology Division, Oak Ridge National Laboratory, Oak Ridge, Tennessee 37831, USA. [5]Department of Materials Science and Engineering, University of Tennessee, Knoxville, Tennessee 37996, USA. [6]Department of Physics and Astronomy, University of Tennessee, Knoxville, Tennessee 37996, USA. [7]Department of Materials Science and Engineering, University of Washington, Seattle, Washington 98195, USA.
*e-mail: wangyao@hku.hk; xuxd@uw.edu

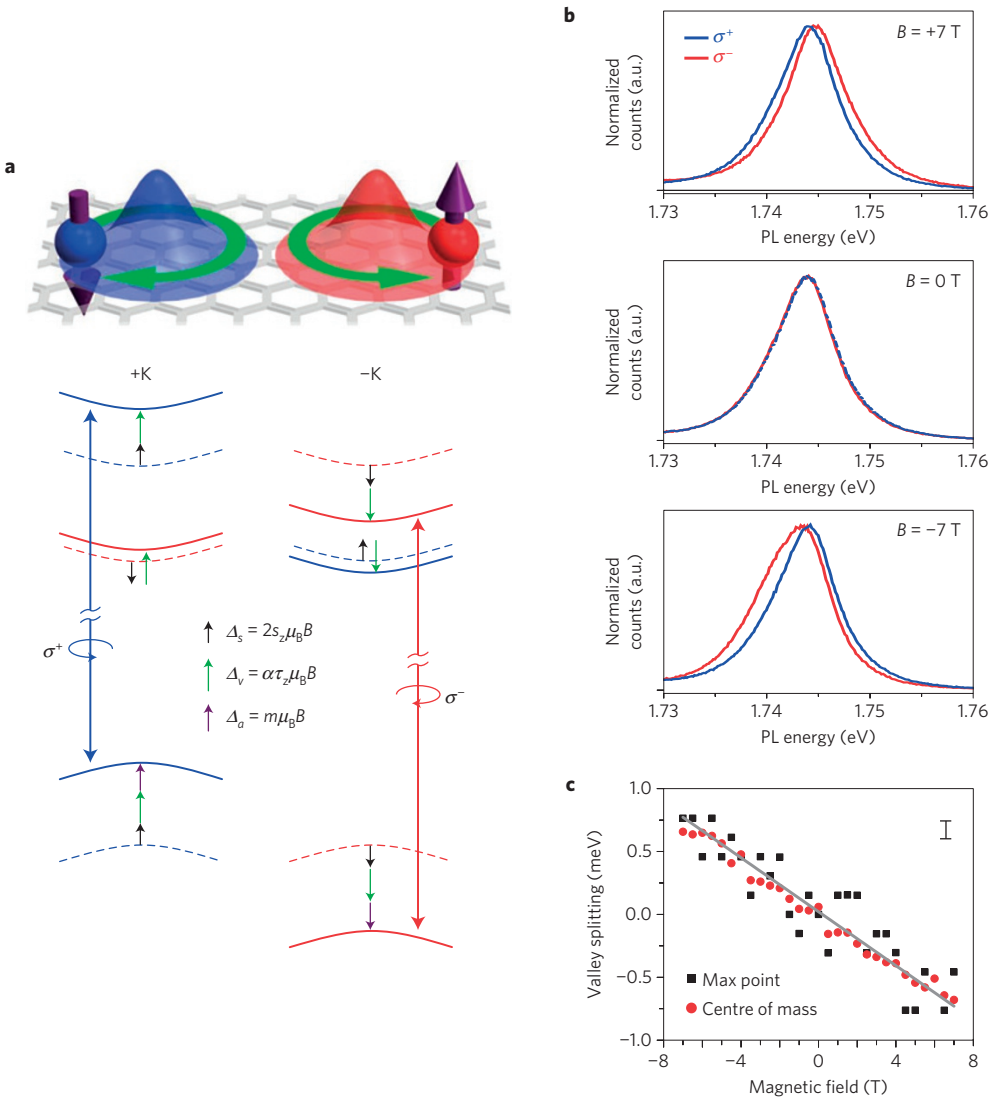

Figure 1 | Valley Zeeman splitting. a, Top: cartoon depicting the valley magnetic moments. Blue (red) represents spin up (down) in +K (−K) valleys. The self-rotation of the wavepacket indicated by green arrows gives rise to the valley magnetic moment. For holes, the magnetic moment also has a contribution from the atomic orbital (purple arrow), which has opposite sign in the K and −K valleys. Bottom: energy level diagram showing the three contributions to the valley Zeeman shifts (black for spin, green for valley, purple for atomic orbital). See text for explanation. **b**, Polarization-resolved valley-exciton photoluminescence (PL) at selected magnetic fields. Blue and red curves represents PL when exciting and detecting with a single helicity, corresponding to the +K and −K valleys, respectively. **c**, Valley-exciton Zeeman splitting as a function of magnetic field extracted using two different methods, as described in the Supplementary Methods. The solid line is a linear fit (to the black squares) using the equation described in the text. The bar at the top right indicates the spectral resolution of the detection system.

the two valleys[26,27], and both spin states are relevant. The overall Zeeman shift of each band is determined by the sum of these three contributions to magnetic moment, which leads to an effective g-factor different from the vacuum value of 2.

The Zeeman shift due to the spin magnetic moment ($\Delta_s = 2s_z\mu_B B$, black arrows) does not affect the optical resonances because optical transitions conserve spin so that the effect on the initial and final states is the same. The atomic orbital contribution, however, does affect them because the conduction band edges are mainly composed of d-orbitals with $m = 0$, whereas the valence band edges are mainly d-orbitals with $m = 2$ in the +K valley and $m = -2$ in the −K valley. This contributes no shift to the conduction band and a shift of $\Delta_\alpha = 2\tau\mu_B B$ to the valence band edge (purple arrows), resulting in a net shift of the optical resonances by $-2\tau\mu_B B$, where $\tau = \pm 1$ is the index for the ±K valleys.

The Zeeman shift due to the valley magnetic moment is $\Delta_v = m_\tau B$ (green arrows), with $m_\tau = \alpha_i\tau\mu_B$, where α_i is the valley g-factor for band i ($i = c, v$). The leading order $\mathbf{k}\cdot\mathbf{p}$ approximation for the band-edge carriers yields a massive Dirac fermion model[1,6] with $\alpha = (m_0/m^*)$, where m^* is the effective mass, which is the same for both conduction and valence bands[1]. Within this approximation, the valley magnetic moment therefore does not affect the exciton resonances, just as for the bare spin. However, corrections beyond leading order give different effective masses and different valley magnetic moments for the electrons and holes[26–28]. The result is a valley-dependent shift of the optical resonances by $\tau\Delta\alpha\mu_B B$, where $\Delta\alpha = \alpha_c - \alpha_v$.

The net effect is a valley-dependent linear shift of the exciton resonance by $-\tau\Delta(B)/2$, where $\Delta(B) = 2(2 - \Delta\alpha)\mu_B B$ is the excitonic valley Zeeman splitting. Thus the +K valley exciton ($\tau = 1$) should be redshifted with respect to the −K valley exciton ($\tau = -1$) for $B > 0$, and blueshifted for $B < 0$, consistent with the observations in Fig. 1b. The best fit to the data (grey line) in Fig. 1c yields $\Delta\alpha = 1.1 \pm 0.1$. The average value of $\Delta\alpha$ found over five similar

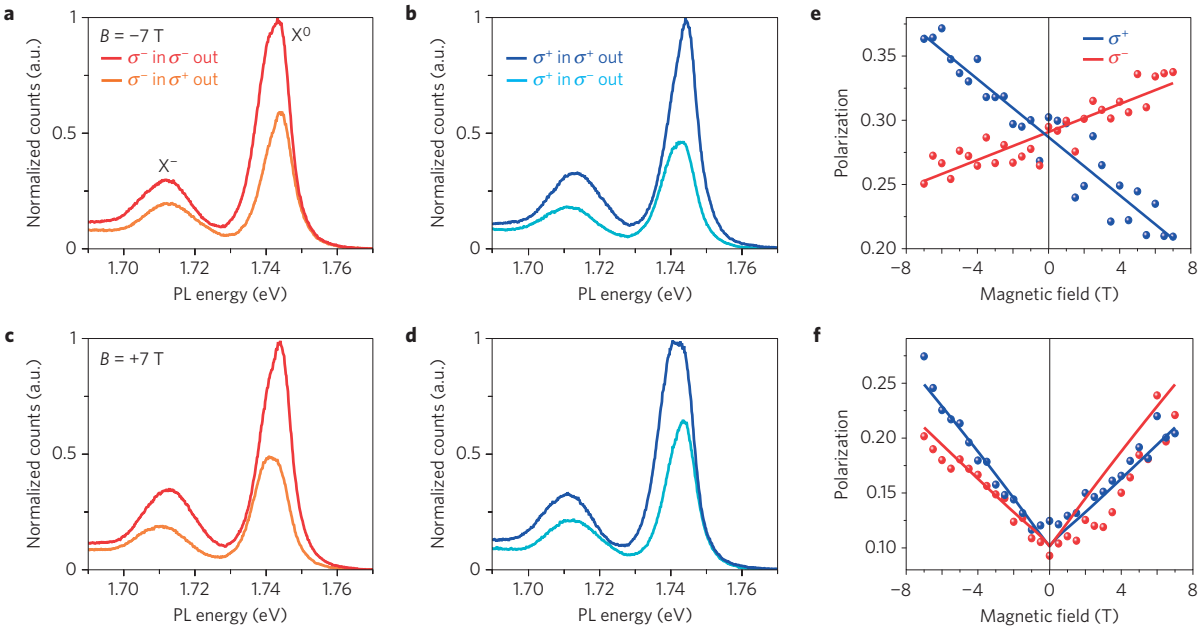

Figure 2 | Magnetic tuning of valley polarization. a–d, Polarization-resolved photoluminescence (PL) showing the asymmetric valley pseudospin relaxation at magnetic fields of −7 T (**a**,**b**) and +7 T (**c**,**d**). **a**,**c**, For σ^- excitation with detection by σ^- (red) and σ^+ (orange) polarization. **b**,**d**, For σ^+ excitation and detection by σ^+ (blue) and σ^- (light blue) polarization. **e**,**f**, Degree of photoluminescence polarization for exciton and trion peaks, respectively. Blue (red) represents σ^+ (σ^-) excitation. Lines are fits using the models described in Supplementary Methods 5 and 6.

samples was 1.2. We note that there are some variations between samples (Supplementary Methods 1), which can be separated into two groups with mean splittings of 1.57 μB and 2.86 μB. The origin of this bimodal distribution in the g-factors is unclear owing to the lack of understanding of what external factors can affect the g-factors in these new materials. Future studies will be necessary to quantitatively determine the effect of variables such as strain, doping and substrate on the magnetic properties. Nevertheless, this measurement of a definite non-zero $\Delta\alpha$ directly implies the existence of finite valley magnetic moments (and therefore finite Berry curvature), in addition to a deviation from the massive Dirac fermion model (Supplementary Methods 2).

The splitting in the applied magnetic field breaks the valley degeneracy, enabling control of the valley polarization. To investigate this we measure the degree of PL polarization for both helicities of incident circular polarization. Figure 2a shows PL for σ^- excitation with σ^- (red) and σ^+ (orange) detection at a field of −7 T. The suppression of the σ^+ signal relative to the co-polarized σ^- peak is a signature of optically pumped valley polarization[7–10]. The degree of exciton valley polarization is clearly larger for σ^+ excitation than for σ^- excitation (Fig. 2b). On the other hand, when the magnetic field is reversed to +7 T (Fig. 2c,d) the polarization becomes larger for σ^-. This observation implies that, whereas the sign of the valley polarization is determined by the helicity of the excitation laser, its magnitude depends on the relationship between the helicity and the magnetic field direction.

Figure 2e shows the degree of PL polarization for both σ^+ (blue) and σ^- (red) excitation as a function of B between −7 T and +7 T for the neutral exciton peak. It is linear in B, with a negative (positive) slope. This 'X' pattern implies that the valley Zeeman splitting induces an asymmetry in the intervalley scattering. (Note that the overall tilt of the 'X' pattern seen here signifies an asymmetry of the response of the entire experimental system to magnetic field whose origin we do not know, but it does not affect any of our conclusions.) In contrast, the PL polarization of the negative trion peak increases for either sign of B and shows a 'V' pattern (Fig. 2f).

These findings can be understood as resulting from magnetic tuning of the different dispersions of valley excitons and trions, as illustrated in Fig. 3. Exchange interactions between electrons and holes strongly couple the valley pseudospin to the exciton centre-of-mass wavevector $\mathbf{k}$, splitting the exciton dispersion into two branches (Supplementary Methods 3 and 4; ref. 25). As shown in Fig. 3a, the upper branch has a steeper dispersion: its states have much smaller momenta than states at the same energy on the lower branch (Fig. 3a). At $B=0$, the two branches touch at $\mathbf{k}=0$, where the two degenerate eigenstates are the −K and +K valley excitons, which emit σ^- and σ^+ light, respectively (Fig. 3a, middle). A finite magnetic field lifts this degeneracy and opens a gap $\Delta(B)$. For $B>0$ the centres of the upper and lower branches are the −K and +K valley excitons respectively[25] (Fig. 3a, right). For $B<0$ these are interchanged (Fig. 3a, left).

The 'X' pattern for neutral excitons results from the fact that the formation of σ^- excitons for $B>0$ and σ^+ excitons for $B<0$ is much easier because of the magnetic tuning of excitonic dispersion. At $B>0$ with σ^+ excitation (Fig. 3b), electrons and holes are created at $\mathbf{k}=0$ in the +K valley and relax to form +K excitons (blue, centre of lower exciton branch) at a valley-conserving rate γ_1 or −K excitons (red, centre of upper branch) at a valley-flipping rate γ_2. For σ^- excitation (Fig. 3c), the valley-conserving and valley-flipping processes result in −K and +K valley excitons, respectively, instead. The degree of PL polarization is determined by valley depolarization both during exciton formation (that is, the ratio γ_2/γ_1) and in the exciton ground state before recombination (r_1). The measurements in Fig. 2a–d illustrate our finding that in all cases the higher-energy exciton retains more valley polarization than the lower-energy exciton. This is the opposite of what would result from thermal relaxation to the lowest-energy valley-exciton state. It implies that the PL polarization is largely determined during the exciton formation process.

The steeper dispersion of the upper exciton branch should facilitate formation of excitons in this branch relative to those in the lower branch, in which larger momentum transfers by scattering are required to reach the light cone (see Supplementary Fig. 2). Therefore, for $B>0$, the carriers created by σ^- excitation have a larger valley-conserving rate γ_1 and a smaller valley-flipping rate γ_2 than for σ^+, leading to $\gamma_1(\sigma^-)/\gamma_2(\sigma^-) > \gamma_1(\sigma^+)/\gamma_2(\sigma^+)$ and

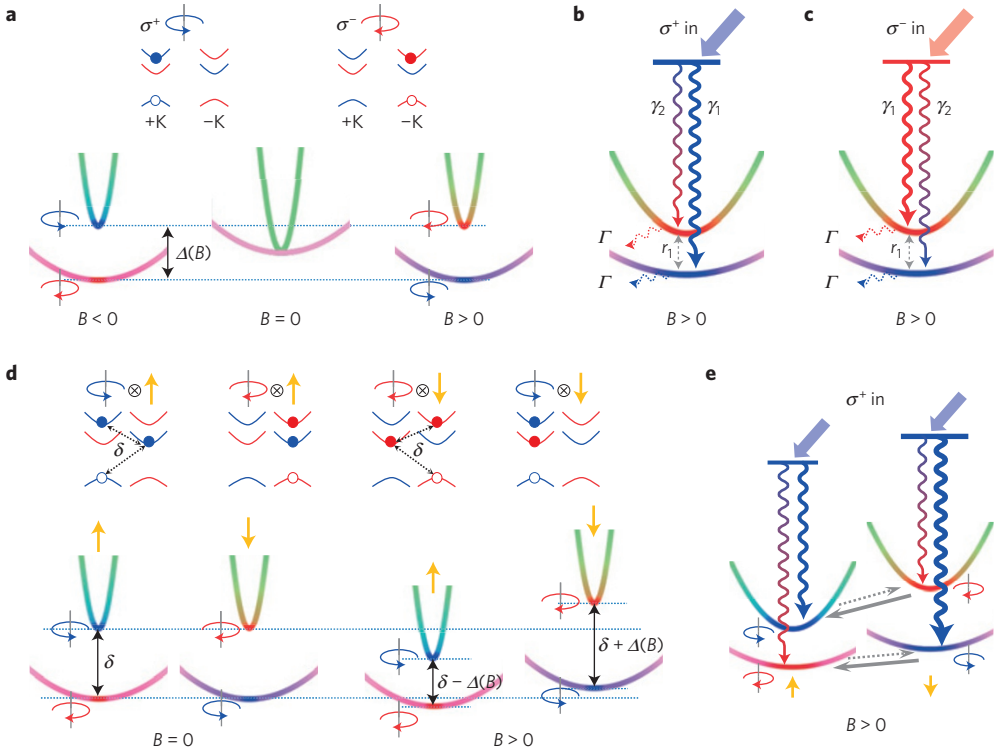

Figure 3 | Valley exciton and trion energy spectra in a magnetic field. a, Top: Valley excitons formed at the band edges at K and −K, which emit σ^+ and σ^- polarized light respectively. Spin-up (down) bands are shown in blue (red). Bottom: valley–orbit coupled exciton energy spectrum with and without a magnetic field. The colour here indicates the valley pseudospin configuration: blue (red) denotes valley K (−K), and green and purple represent superpositions of K and −K. **b**,**c**, Cartoons depicting asymmetric valley-conserving (γ_1; thick wavy lines in single colour) and valley-flipping (γ_2; thin wavy lines with colour gradient) exciton formation processes under σ^+ (**b**) and σ^- (**c**) excitation, with r_1 showing exciton ground recombination. See text for explanation. **d**, Top: four configurations of bright trion X^- labelled with the valley polarization and spin orientation of the extra electron. Bottom: trion dispersion with an exchange-induced gap (δ) at $\mathbf{k}=0$ with (right) and without (left) magnetic field. **e**, Cartoon showing asymmetric valley-conserving and valley-flipping formation of the bright trion states in a magnetic field. Solid and dashed arrows indicate intervalley scattering by emitting energy to and absorbing energy from the environment, respectively. See text for details.

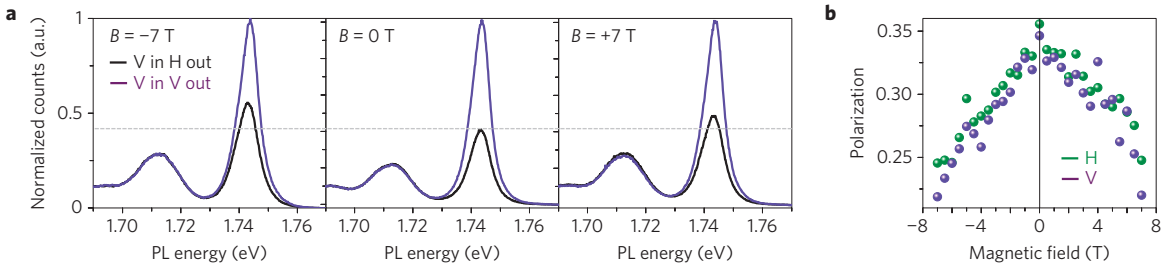

Figure 4 | Magnetic control of valley coherence. a, Polarization-resolved photoluminescence (PL) at −7 T (left), 0 T (middle) and +7 T (right) by vertically polarized excitation. Purple and black curves represent vertically and horizontally polarized detection, respectively. **b**, Degree of linear polarization as a function of magnetic field. Green and purple dots denote horizontally and vertically polarized excitation, respectively.

a larger valley polarization, as observed. For $B<0$ the converse holds by time-reversal symmetry. By solving the rate equations, taking the field-dependent valley-exciton formation process and measured valley Zeeman splitting (Fig. 1c) into account, the 'X' pattern can be fully reproduced, as shown by the solid lines in Fig. 2e (Supplementary Methods 5).

Within the same framework, the 'V' pattern seen for negative trions (X^-) can also be explained as resulting from their qualitatively different spectrum. With a second electron occupying either the lowest-energy spin-up band in the +K valley or spin-down band in the −K valley (top panel, Fig. 3d), at $B=0$, X^- has two degenerate sets of valley–orbit coupled bands where the large exchange interaction with the extra electron opens a gap δ (~6 meV; ref. 25) at $\mathbf{k}=0$ (bottom panel, Fig. 3d). As δ is already much larger than the achievable valley Zeeman splitting, the asymmetry in valley-exciton formation rates in the presence of a field does not dominate the B dependence of the X^- valley polarization. Instead, the valley Zeeman splitting breaks the energy degeneracy of the X^- ground states, which suppresses the valley relaxation channels (grey arrows in Fig. 3e) relative to their zero-field rates. This mechanism protects the valley polarization and increases the PL polarization for either sign of B. Taking into account the valley depolarization in the exciton formation process, as in the neutral exciton case, we can reproduce the 'V' pattern of X^- valley polarization, the result being the solid lines in Fig. 2f (Supplementary Methods 5 and 6).

Simply put, the difference between the 'X' and 'V' patterns reflects the different dominant valley depolarization process. If depolarization occurs during exciton formation, one sees an 'X'

pattern because exciton formation favours the upper exciton branch. If, on the other hand, depolarization occurs predominantly after reaching the ground state, one sees a 'V' shape because either sign of magnetic field suppresses the ground-state inter-valley relaxation.

Finally, we investigate the magnetic field dependence of valley coherence. Figure 4a shows the polarization-resolved PL spectrum at selected fields with vertically polarized excitation and vertically (purple) and horizontally (black) polarized detection. As shown previously[10], the observed linear polarization of the exciton PL is due to the creation of valley quantum coherence. As the magnetic field increases, the degree of linear polarization decreases and shows a 'Λ' pattern (Fig. 4b). This demonstrates that valley coherence is suppressed by magnetic field. The data for horizontally polarized excitation is also plotted, showing that the effect is isotropic and not due to any crystal anisotropy.

Like depolarization, valley decoherence can occur during both the exciton formation and its ground-state recombination processes. The magnetic field dependence in the latter case is the Hanle effect, in which spin precession quenches the linear polarization, and the half-width of the Hanle peak corresponds to the decoherence rate. Here, the linearly polarized exciton has an in-plane valley pseudospin. The Hanle effect is qualitatively consistent with the 'Λ' pattern observed; however, the extracted valley decoherence and the exciton recombination times are both of the order of 1 ps (Supplementary Methods 7), which is much smaller than those deduced from time-resolved measurements[17]. It is therefore likely that valley pseudospin precession and decoherence in the exciton formation process dominate. After linearly polarized excitation generates electron–hole pairs in a superposition of the two valleys, the +K and −K valley-exciton formation pathways (the red and blue wavy lines in Fig. 3b) become different as the magnetic field opens the gap (as inferred from the polarization data in Fig. 2e). This difference destroys the optically generated coherence during the formation of ground-state excitons, leading to reduced linear polarization of the PL.

During preparation of manuscript, we became aware of similar work on WSe_2 by the ETH group[28] and on $MoSe_2$ by the Cornell group[29].

Methods

A monolayer sample of WSe_2 is mechanically exfoliated onto 300 nm SiO_2 on heavily doped Si. The samples are cooled typically to 30 K in a closed-cycle cryostat with a 7 T superconducting magnet in the Faraday geometry. The samples are excited with a 1.88 eV laser focused to a 2 μm spot size with an aspheric lens. The photoluminescence was collected with same lens and free-space coupled to a spectrometer with a liquid nitrogen cooled CCD detector.

Received 7 July 2014; accepted 19 November 2014; published online 26 January 2015

References

1. Xu, X., Yao, W., Xiao, D. & Heinz, T. F. Spin and pseudospins in layered transition metal dichalcogenides. *Nature Phys.* **10,** 343–350 (2014).
2. Zhu, Z., Collaudin, A., Fauque, B., Kang, W. & Behnia, K. Field-induced polarization of Dirac valleys in bismuth. *Nature Phys.* **8,** 89–94 (2012).
3. Rycerz, A., Tworzydlo, J. & Beenakker, C. W. J. Valley filter and valley valve in graphene. *Nature Phys.* **3,** 172–175 (2007).
4. Gunawan, O. *et al.* Valley susceptibility of an interacting two-dimensional electron system. *Phys. Rev. Lett.* **97,** 186404 (2006).
5. Gunawan, O., Habib, B., De Poortere, E. P. & Shayegan, M. Quantized conductance in an AlAs two-dimensional electron system quantum point contact. *Phys. Rev. B* **74,** 155436 (2006).
6. Xiao, D., Liu, G-B., Feng, W., Xu, X. & Yao, W. Coupled spin and valley physics in monolayers of MoS_2 and other group-VI dichalcogenides. *Phys. Rev. Lett.* **108,** 196802 (2012).
7. Zeng, H., Dai, J., Yao, W., Xiao, D. & Cui, X. Valley polarization in MoS_2 monolayers by optical pumping. *Nature Nanotech.* **7,** 490–493 (2012).
8. Cao, T. *et al.* Valley-selective circular dichroism of monolayer molybdenum disulphide. *Nature Commun.* **3,** 887 (2012).
9. Mak, K. F., He, K., Shan, J. & Heinz, T. F. Control of valley polarization in monolayer MoS_2 by optical helicity. *Nature Nanotech.* **7,** 494–498 (2012).
10. Jones, A. M. *et al.* Optical generation of excitonic valley coherence in monolayer WSe_2. *Nature Nanotech.* **8,** 634–638 (2013).
11. Mak, K. F., McGill, K. L., Park, J. & McEuen, P. L. The valley Hall effect in MoS_2 transistors. *Science* **344,** 1489–1492 (2014).
12. Li, X., Zhang, F. & Niu, Q. Unconventional quantum Hall effect and tunable spin Hall effect in Dirac materials: Application to an isolated MoS_2 trilayer. *Phys. Rev. Lett.* **110,** 066803 (2013).
13. Chu, R-L. *et al.* Valley-splitting and valley-dependent inter-Landau-level optical transitions in monolayer MoS_2 quantum Hall systems. *Phys. Rev. B* **90,** 045427 (2014).
14. Jones, A. M. *et al.* Spin-layer locking effects in optical orientation of exciton spin in bilayer WSe_2. *Nature Phys.* **10,** 130–134 (2014).
15. Wu, S. *et al.* Electrical tuning of valley magnetic moment through symmetry control in bilayer MoS_2. *Nature Phys.* **9,** 149–153 (2013).
16. Lagarde, D. *et al.* Carrier and polarization dynamics in monolayer MoS_2. *Phys. Rev. Lett.* **112,** 047401 (2014).
17. Wang, G. *et al.* Valley dynamics probed through charged and neutral exciton emission in monolayer WSe_2. *Phys. Rev. B* **90,** 075413 (2014).
18. Wang, G. *et al.* Non-linear optical spectroscopy of excited exciton states for efficient valley coherence generation in WSe_2 monolayers. Preprint at http://arxiv.org/abs/1404.0056 (2014).
19. Zhu, B., Chen, X. & Cui, X. Exciton binding energy of monolayer WS_2. Preprint at http://arxiv.org/abs/1403.5108 (2014).
20. Zhang, C., Johnson, A., Hsu, C-L., Li, L-J. & Shih, C-K. Direct imaging of band profile in single layer MoS_2 on graphite: Quasiparticle energy gap, metallic edge states, and edge band bending. *Nano Lett.* **14,** 2443–2447 (2014).
21. Ye, Z. *et al.* Probing excitonic dark states in single-layer tungsten disulphide. *Nature* **513,** 214–218 (2014).
22. Chernikov, A. *et al.* Exciton binding energy and nonhydrogenic Rydberg series in monolayer WS_2. *Phys. Rev. Lett.* **113,** 076802 (2014).
23. He, K. *et al.* Tightly bound excitons in monolayer WSe_2. *Phys. Rev. Lett.* **113,** 026803 (2014).
24. Ugeda, M. M. *et al.* Giant bandgap renormalization and excitonic effects in a monolayer transition metal dichalcogenide semiconductor. *Nature Mater.* **13,** 1091–1095 (2014).
25. Yu, H., Liu, G-B., Gong, P., Xu, X. & Yao, W. Dirac cones and Dirac saddle points of bright excitons in monolayer transition metal dichalcogenides. *Nature Commun.* **5,** 3876 (2014).
26. Liu, G-B., Shan, W-Y., Yao, Y., Yao, W. & Xiao, D. Three-band tight-binding model for monolayers of group-VIB transition metal dichalcogenides. *Phys. Rev. B* **88,** 085433 (2013).
27. Kormányos, A. *et al.* Monolayer MoS_2: Trigonal warping, the Γ valley, and spin–orbit coupling effects. *Phys. Rev. B* **88,** 045416 (2013).
28. Srivastava, A. *et al.* Valley Zeeman effect in elementary optical excitations of a monolayer WSe_2. Preprint at http://arxiv.org/abs/1407.2624 (2014).
29. MacNeill, D. *et al.* Valley degeneracy breaking by magnetic field in monolayer $MoSe_2$. Preprint at http://arxiv.org/abs/1407.0686 (2014).

Acknowledgements

We thank X. Li for helpful discussions. This work is mainly supported by the DoE, BES, Materials Sciences and Engineering Division (DE-SC0008145). Z.G. and W.Y. were supported by the Croucher Foundation (Croucher Innovation Award) and the RGC of Hong Kong (HKU705513P, HKU9/CRF/13G). D.C. is supported by US DoE, BES, Materials Sciences and Engineering Division (DE-SC0002197). J.Y. and D.G.M. were supported by US DoE, BES, Materials Sciences and Engineering Division. R-L.C. and C.Z. are supported by ARO (W911NF-12-1-0334) and AFOSR (FA9550-13-1-0045). X.X. acknowledges a Cottrell Scholar Award. Device fabrication was performed at the University of Washington Microfabrication Facility and NSF-funded Nanotech User Facility.

Author contributions

X.X. and W.Y. conceived the project; G.A. performed the experiment, assisted by A.M.J., under the supervision of X.X.; G.A. and X.X. analysed the data; Z.G. and W.Y. provided the theoretical explanation, with input from R-L.C. and C.Z.; J.Y. and D.G.M. synthesized and characterized the bulk WSe_2 crystals; G.A., X.X., W.Y., D.C. and Z.G. wrote the paper. All authors discussed the results.

Additional information

Supplementary information is available in the online version of the paper. Reprints and permissions information is available online at www.nature.com/reprints. Correspondence and requests for materials should be addressed to W.Y. or X.X.

Competing financial interests

The authors declare no competing financial interests.